Numerical simulation of time-dependent fracture of graded bimaterial metallic interfaces

ALI P. GORDON[1] and DAVID L. MCDOWELL[1,2]
[1]*The George W. Woodruff School of Mechanical Engineering, Georgia Institute of Technology, Atlanta, GA 30332-0405 U.S.A.*
[2]*School of Materials Science and Engineering, Georgia Institute of Technology, Atlanta, GA 30332-0230 U.S.A.*

Abstract. Stationary cracks along and near interfaces between two time-dependent materials are simulated using the finite element method (FEM) to examine crack tip fields and candidate driving force parameters for crack growth. Plane strain conditions are assumed. In some cases, a thin transition layer is included between the two materials. This transition layer features a functionally graded blend of properties of the two materials. An example of such a system is that of weld metal (WM) and base metal (BM) in a weldment, with the transition layer corresponding to the heat-affected zone (HAZ). Numerical solutions for the stress and strain fields of homogeneous and heterogeneous Compact Tension (C(T)-type) specimens are presented. The equivalent domain integral technique is employed to compute the J-integral for elastic-plastic cases as well as the $C(t)$-integral and transition times for creep behavior. Results from parametric studies are curve-fit in terms of transition layer thickness and crack position, inelastic property mismatches, and other independent model parameters. Results indicate that the incorporation of functionally graded transition layer regions leads to less concentrated stress and strain components along interfaces ahead of the crack tip. It is also shown that the computed fracture parameters are influenced by the transition layer properties.

Key words: Bimaterials, creep, finite elements, functionally graded interphases, interfaces, weldment.

Nomenclature

α	= work hardening regression constant
δ_{ij}	= identity tensor
ε_{ij}	= strain tensor
$\bar{\varepsilon}$	= effective strain
ε_o	= reference strain
Γ	= path of line integral
ν	= Poisson's Ratio
σ_{ij}	= stress tensor (MPa)
σ'_{ij}	= stress deviator (MPa)
σ_o	= reference stress (MPa)
$\bar{\sigma}$	= effective stress (MPa)

σ_m = mean or hydrostatic stress (MPa)

A = Norton creep hardening coefficient (MPa^{-n}hr^{-1})

a = crack size (mm)

B = C(T) specimen depth (mm)

BM = base metal region

C^* = steady-state creep domain integral (MPa-mm/hr)

$C(t)$ = Path-dependent creep domain integral (MPa-mm/hr)

E = elastic modulus (MPa)

e = weld line eccentricity (mm)

HAZ = heat-affected zone region

I_m, I_n = integration constants

J = J-integral (MPa-mm)

K_I = Mode I stress intensity factor (MPa-mm$^{\frac{1}{2}}$)

M_p = mode mixity parameter

m = Ramberg-Osgood strain hardening exponent

n = Norton creep strain hardening exponent

P = applied load (N)

r = distance from the crack tip (mm)

t = transition layer thickness (mm)

t_T = transition time in creep case (hr)

u_i = displacement field

W^e = strain energy density (MPa)

W^* = strain energy rate density in creep case (MPa/hr)

W = C(T) specimen width (mm)

WM = weld metal region

1. Introduction

Several microstructural mechanisms influence creep deformation near the crack tip. When polycrystalline materials, such as creep-ductile CrMoV steels, are exposed to elevated temperature conditions, grain boundary sliding and void coalescence can lead to macroscopic fracture. In temperature-resistant, directionally-solidified Nickel-base alloys, deformation is due to the accumulation of time-dependent inelastic shear strains on preferred crystallographic slip planes. Structures fabricated from these materials can include discrete or gradual property variation, which necessitates the consideration of the interfacial fracture toughness.

Interfacial fracture mechanics developments cover a variety length scales and focus on different material behavior regimes. The number of practical applications for interface fracture analyses has proliferated over the last 15 years; however, usable results related to interfaces with non-negligible yield zones and crack tip propagation are still limited. This is due to the lack of understanding the fundamental relationships between interfacial crack tip driving forces and structural attributes that resist these forces.

The purpose of this investigation is to compare crack tip parameters of welded bimaterial specimens with time-dependent mechanical properties. We assume that the cracked bodies are subjected to remote loads that are opening mode-dominated. We consider bimaterial specimens with the crack either along or parallel to the interface. Material properties are varied along with crack face-to-interface distance. Results are compared to the case of homogeneous material specimens. We then discuss bimaterial fracture and creep problems in the presence of a transition layer in the context of a weldment with a base metal (BM), weld metal (WM) and heat-affected zone (HAZ), all with different plasticity and creep behaviors, but with matched isotropic linear elastic behavior. Analysis of the stress, strain, and displacement fields near the stationary crack tip permits assessment of the conditions for crack extension along the interface as well as crack kinking.

2.   Crack tip driving forces

2.1.   HOMOGENEOUS CRACKED BODIES

Many bonded structural components are comprised of constituents with dissimilar material properties. Several common examples are rock-concrete abutments at dam bases, chip-solder-substrate structures in electronic interconnects, and welded pressure vessel and piping components in elevated temperature power generation applications. Each of these applications represents a situation in which failure due to interface fracture is a limiting consideration.

The solution of the homogeneous cracked body is well-documented (Bassani et al., 1981; Hutchinson, 1968; Riedel and Rice, 1980; Rice, 1968; Saxena, 1998; Shih, 1974). Elastic, elastic-plastic, or elastic-creep, solutions have been derived for elastic, elastic-plastic, or elastic-creep conditions to describe the stress, strain, and displacement fields ahead of a crack tip. For a Compact Tension (C(T)-type) fracture specimen of thickness B, size W, and initial crack length a, the Mode I stress intensity factor is given by

$$K_I = \frac{P}{B\sqrt{W}} F\left(\frac{a}{W}\right), \tag{1}$$

where F is the dimensionless geometric factor given by Tada et al. (1985). Of course K_I still applies to the case of small scale yielding at the crack tip. For large scale time-independent yielding at the crack tip, the J-integral is defined by (Rice, 1968)

$$J = \int_{\Gamma} W^e dy - T_i \frac{\partial u_i}{\partial x} ds, \tag{2}$$

where $W^e = \int \sigma_{ij} d\varepsilon_{ij}$. The J-integral corresponds to the rate of potential energy release due to crack extension in an equivalent non-linear elastic body. Assuming that the inelastic strain of the material obeys the Ramberg-Osgood law for work hardening for proportional loading,

$$\varepsilon_{ij} = \frac{1+\nu}{e}\sigma_{ij} - \frac{\nu}{E}\sigma_{kk}\delta_{ij} + \frac{3}{2}\alpha\left(\frac{\bar{\sigma}}{\sigma_o}\right)^{m-1}\frac{\sigma_{ij}'}{E}, \tag{3}$$

where E and ν are elastic constants, and α, σ_o, and m are power law plasticity constants. The deviatoric and effective stresses are defined as $\sigma_{ij}' = \sigma_{ij} - \frac{1}{3}\sigma_{kk}\delta_{ij}$ and $\bar{\sigma} = \sqrt{\frac{3}{2}\sigma_{ij}'\sigma_{ij}'}$, respectively. The J-integral parameterizes the HRR stress and strain fields for small scale yielding given as (Hutchinson, 1968)

$$\sigma_{ij} = \sigma_o \left(\frac{J}{\alpha \sigma_o \varepsilon_o I_m r} \right)^{\frac{1}{m+1}} \hat{\sigma}_{ij}^I(\theta, m), \quad \varepsilon_{ij}^p = \alpha \varepsilon_o \left(\frac{J}{\alpha \sigma_o \varepsilon_o I_m r} \right)^{\frac{m}{m+1}} \hat{\varepsilon}_{ij}^I(\theta, m), \tag{4}$$

where ε_o is the reference strain, usually corresponding to the point of initial yield, I_m is an integration constant, r and θ are crack tip polar coordinates, and $\hat{\sigma}_{ij}^I$ and $\hat{\varepsilon}_{ij}^I$ are angular-dependent functions. Equation (4) is exact in the fully plastic limit and is approximately correct for small-scale yielding.

For time-dependent material behavior, Landes and Begley (1976) and Nikbin et al. (1976) independently proposed the C^*-integral as the analogous fracture parameter for extensive steady state creep (EC) conditions, defined by

$$C^* = \int_\Gamma W^* dy - T_i \frac{\partial \dot{u}_i}{\partial x} ds, \tag{5}$$

where $W^* = \int \sigma_{ij} d\dot{\varepsilon}_{ij}$. The C^*-integral, an extension of the J-integral, is used to describe the crack tip fields under extensive creep deformation, i.e., steady state creep conditions must exist throughout the entire body. Under a multiaxial stress state and steady state creep conditions, the material is assumed to follow Norton's creep law, i.e.,

$$\dot{\varepsilon}_{ij} = \frac{1+\nu}{E} \dot{\sigma}_{ij} - \frac{\nu}{E} \dot{\sigma}_{kk} \delta_{ij} + \frac{3}{2} A \bar{\sigma}^n \left(\frac{\sigma_{ij}'}{\bar{\sigma}} \right) \tag{6}$$

The stress and strain rate fields near the crack tip are given as (Hutchinson 1968; Rice and Rosengren, 1968)

$$\sigma_{ij} = \left(\frac{C^*}{A I_n r} \right)^{\frac{1}{n+1}} \hat{\sigma}_{ij}^I(\theta, n), \quad \dot{\varepsilon}_{ij}^c = A \left(\frac{C^*}{A I_n r} \right)^{\frac{1}{n+1}} \hat{\varepsilon}_{ij}^I(\theta, n) \tag{7}$$

Here, I_n is an integration constant based on the creep strain exponent, n, approximated under plane strain conditions (Saxena, 1998). The angular dependent functions in each expression, $\hat{\varepsilon}_{ij}^I$ and $\hat{\sigma}_{ij}^I$, depend only on material property n and location around the crack tip, are identical to those in Equation (4). To address the small scale, transient behavior prior to reaching extensive steady state creep conditions, Bassani and McClintock (1981) introduced the path-dependent crack tip singularity amplitude $C(t)$-integral

$$C(t) = \int_{\substack{\Gamma \\ \lim_{r \to 0}}} W^* dy - T_i \frac{\partial \dot{u}_i}{\partial x} ds \tag{8}$$

This expression is defined within the region where effective elastic strains are dominated by the effective creep strains. This is true only very near the crack tip upon initial loading. Under plane strain, K_I-dominated small scale creep conditions (SSC), $C(t)$ can be approximated by (Ehlers and Riedel, 1991)

$$C(t) = \frac{K_I^2(1 - \nu^2)}{E(n+1)t} \tag{9}$$

Under EC conditions, $C(t)$ becomes path-independent and equivalent to C^*. We may interpolate between SSC and EC conditions to obtain the complete approximation (Saxena, 1998)

$$C(t) = \frac{K_I^2(1 - \nu^2)}{E(n+1)t} + C^* \tag{10}$$

The transition from SSC to EC conditions is designated by the transition time, t_T, and is defined when $C(t)$ is twice C^*. As such, the transition times for homogeneous models of the base metal (BM), weld metal (WM), and heat-affected zone metal (HAZ) are denoted as t_{TBM}, t_{TWM}, and t_{THAZ}, respectively. The divergence theorem was applied to Equations (2) and (8) to obtain the domain integral formulations of J and $C(t)$, i.e.,

$$J = \int_{A_\Gamma} [-W^e \delta_{1j} + \sigma_{ij} u_{i,1}] q_{1,j} dA_\Gamma, \; C(t) = \int_{A_{\Gamma \to 0}} [-W^e \delta_{1j} + \sigma_{ij} u_{i,1}] q_{1,j} dA_\Gamma, \qquad (11)$$

where q_1 is an arbitrary smooth function equal to 1 at the crack tip and 0 at the boundary of the domain enclosed by Γ, denoted by A_Γ. Shih and coworkers (1986, 1987) introduced these equivalent domain integrals for accurate, efficient determination of the J- and $C(t)$-integrals using FE models.

2.2. HETEROGENEOUS CRACKED BODIES

In recent studies concerning cracks in bimaterial specimens/bodies (Biner, 1998; Burstow et al., 1998; Francis and Rahman, 2000; Kim and Schwalbe, 2001; Liaw et al., 1989; Luo and Aoki, 1992; Segle et al., 1998; Shih et al., 1991), the effects of mismatch of inelastic properties have been studied, with no elastic mismatch of constituents. As such, certain bimaterial constants introduced by Dundurs (1969) vanish. This simplification is known as the zero-β assumption. As a consequence, the pathologies associated with linear elastic bimaterial interface cracks are removed; however, the techniques used to evaluate the crack tip driving forces are identical.

Investigations have also been conducted for materials with mismatched yield properties following the zero-β assumption. Luo and Aoki (1992) used boundary layer modeling to demonstrate that differences in yield strength do not affect the $r^{-\frac{1}{2}}$ singularity of the near tip fields under small scale yielding conditions, and the lower yield strength, lower work hardening rate material controls the size of the crack tip plastic zone. This was also observed in elastic bimaterials for which larger shear stresses occur in the weaker material. Hydrostatic stresses are larger in this region as well. Kim and Schwalbe (2001) extended this analysis by considering a transition region separating the two materials. This region has averaged mechanical properties of the other two regions. They used various fracture specimens in order to introduce a framework for reliably assessing the life of in-service joined bodies with cracks in the transition layer. They found that deformation is higher in the material with the lower yield strength. For higher property mismatches and/or small transition regions, intense deformation is confined to the lower strength material.

Francis and Rahman (2000) showed that the J-integral for base metal-weld metal-base metal specimens typically fell in the range of the J-integral results for homogeneous specimens of base metal <u>or</u> weld metal. For very thin weld metal regions, fracture behavior approached that of the homogeneous base metal. Conversely, for thick weld regions, contributions of the base metal were minimal and the behavior was similar to the homogeneous weld metal. They linearly interpolated the plastic portion of the J-integral results by using

$$J_p = c\left(\frac{a}{W}, \frac{t}{1.2W}, \chi_{\sigma_0}, \chi_m\right) J_p^{BM} + \left[1 - c\left(\frac{a}{W}, \frac{t}{1.2W}, \chi_{\sigma_0}, \chi_m\right)\right] J_p^{WM}, \qquad (12)$$

where J_p^{BM} and J_p^{WM} are the J-integrals for specimens with same geometry but composed of only homogeneous base or weld metal, respectively. The interpolation factor, c, is based on

geometric variables and property mismatch parameters χ_{σ_0} and χ_m, defined as the weld-to-base metal ratio of any material property, for example $\chi_{\sigma_o} = \sigma_{oWM}/\sigma_{oBM}$. It was later shown by Burstow et al. (1998) that the near tip stress fields are self-similar when normalized by $J/(t\sigma_{0WM})$, where t is the thickness of the weld strip and σ_{0WM} is the yield strength of the weld material.

For elastic-plastic interfaces exposed to dominantly opening mode loading, the near tip stress fields resemble those of the homogenous analogy under mixed mode conditions given as

$$\sigma_{ij} = \sigma_o \left(\frac{J}{\alpha \sigma_o \varepsilon_o I_m r} \right)^{\frac{1}{m+1}} \hat{\sigma}(\theta, M_p, m) \tag{13}$$

The angular-dependent function in this case is parameterized by the plastic mode mixity factor, M_p (Shih, 1977), defined by

$$M_p = \frac{2}{\pi} \tan^{-1} \left(\frac{\sigma_{xy}}{\sigma_{yy}} \right)_{r \to 0} \tag{14}$$

Luo and Aoki (1992) predicted fracture toughness of ductile interfaces using a modified Gurson model to predict initial void volume growth and coalescence based on angular distributions of the hydrostatic and effective stresses. Other micromechanically-based interfacial studies have used a modified Rice-Tracey (R-T) model for spherical void growth (Rice and Tracey, 1969).

2.3. APPLICATION TO WELDMENTS

To relate discussions of a bimaterial interface with a graded transition layer to a physical problem, we consider a weldment as a model system. Weldments are fabricated via high temperature fusion processes. Fused zones influence the strength of the structure. Tailoring the properties in this region minimizes fabrication-induced crack-like flaws and residual stresses and maximizes fracture toughness. Microstructural variation among bodies manufactured with this process causes substantial variability of fracture and creep crack growth (CCG) behaviors. To reduce this variation, reheating and annealing processes are incorporated. Modern fabrication techniques have enhanced control over material arrangement and properties.

Research on weldments has often focused on creep-ductile CrMoV alloys, since fracture specimens can be readily machined from ex-service steam pipe sections. These specimens are subsequently used for CCG and fracture toughness test. For example, Liaw et al. (1989) determined the CCG rates for fused base-weld metal specimens and homogeneous weld metal specimens. CCG rates in creep ductile materials have been well characterized by C_t, introduced by Saxena (1986). In cases where the applied K_I is small, the crack growth rates for fused materials are greater than the weld material for the same K_I. However, when the load is increased, these rates tend to become similar. Large variability in the fracture toughness of heterogeneous specimens was observed. This motivated the need to understand the driving force at the interface. Shih and coworkers addressed this by analyzing the stresses along interfaces in weldment models. This work and subsequent studies (Shih et al., 1991; Shih and Asaro, 1988, 1989; Shih et al., 1993) predicted crack kinking in the direction along the interface of the transition layer and the neighboring material that is more strain compliant – typically the weld metal.
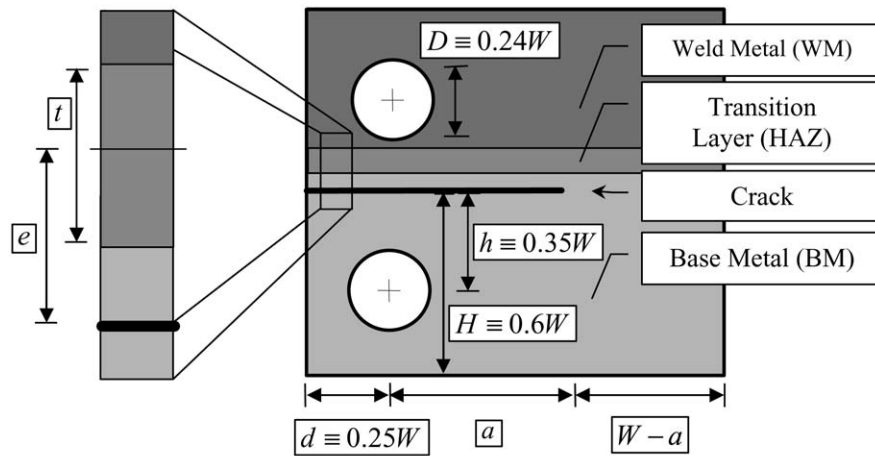
(a)
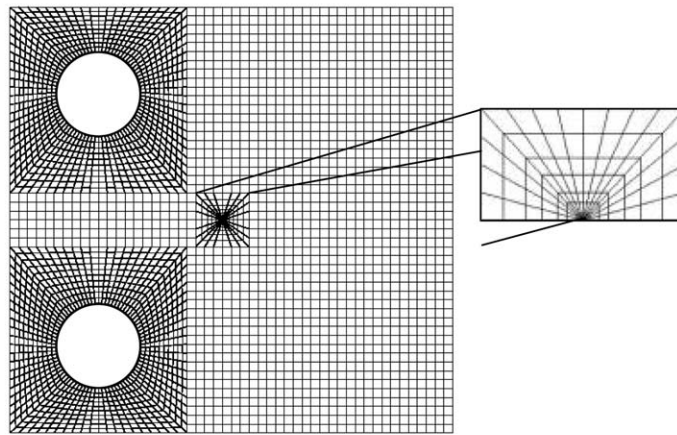
(b)

Figure 1. C(T)-type specimen geometry. (a) Rendering of the numerical heterogeneous bimaterial fracture specimen of HAZ thickness, t, and crack plane eccentricity, e, (measured from the crack plane to the center of the HAZ) and (b) a finite element mesh used in the current investigation.

As shown in Figure 1a, heterogeneous models can incorporate realistic attributes of fracture specimens sectioned from ex-service structures, including the Heat-Affected Zone (HAZ), crack eccentricity, and crack plane-interface angle. Along with obtaining the stress and strain fields at the crack tips of these specimens, some studies predicted initial CCG rates with cavity growth models. Similar to elastic-plastic interface studies, Segle and coworkers (1998) used the modified R-T model (Rice and Tracey, 1969), a creep ductility-based damage relation, to predict initial void link up along the interface. Biner (1998) attempted to predict the crack growth rates in a similar fashion by using a coupled creep deformation and diffusion model developed by Tvergaard (1984). The growth rate of the first cavity ahead of the crack tip was affected by the thickness and the properties of the transition layer. Within the bimaterial structure, the void growth rate is much faster in the lower stiffness material. Because of the
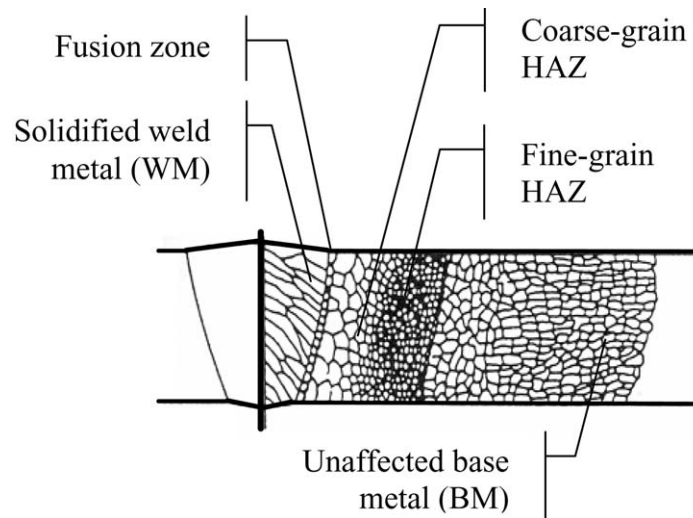
Figure 2. Resulting microstructure around the weld due to back-welding of the base metal (BM).

severe non-proportional loading history experienced at the crack tip, however, their results should only be used for qualitative purposes.

Most time-dependent interfacial fracture studies suggest that void growth and CCG rates are expected to be much higher in bimaterials compared to cracked bodies. Mathematical prediction models for interface crack tip fields in realistic time-dependent materials have not been developed, we extend previously developed techniques to determine fracture parameters of cracks on or near distinct or graded bimaterial interfaces.

3. Numerical simulations

Most existing experimental and analytical results describing fracture parameters and crack tip stress-strain fields are derived using C(T)-type specimens, shown in Figure 1. Although not employed in this study, alternative specimen designs have been used in similar investigations. Examples are the Single-Edge Notched (SEN) specimens (Biner, 1998) and boundary layer formulations (Burstow et al., 1998). The only geometric differences between the experimental C(T)-specimen and our numerical rendering are the 5%W gap used to create the initial notch and the side groove reduction introduced to assist fatigue pre-cracking in laboratory specimens. Our investigation focuses on structures in which the length scale of inelastic deformation at the crack tip is smaller than the thickness of the specimen. This condition is sufficient for plane strain conditions. The far right point of the ligament line on the crack plane was fixed in the y-direction, while the centers of each of the elastic load pins were fixed in the x-direction. This study restricts the specimen size to $W = 25.4$ *mm (1.0 in)*, and crack size to $a = 12.7$ *mm (0.5 in)*. The thickness is $B = 6.35$ *mm (0.25 in)*. For the time-dependent cases the ambient temperature is taken to be $T = 538$ °C. The model geometry is shown in Figure 1b.

Most previous bimaterial fracture models address two distinct perfectly-bonded, isotropic, homogeneous constituents, with the initial crack being coplanar with the interface. The numerical models employed in this study are extensions of those used for the homogeneous case with several modifications. In a typical weldment, models are composed of two bonded homo-

genous, isotropic materials, each occupying either the region above or below the crack plane; however, in cases featuring a HAZ, a graded transition layer is introduced in a region between the homogeneous weld and base metal regions. A weldment that features this type of structure is shown in Figure 2. Two types of loadings configurations were assumed. Each caused either elastic-plastic or elastic-creep crack tip conditions. The material properties corresponding to the material models given in Equations (3) and (6) are given in the next section.

4. Results

4.1. FRACTURE PARAMETERS

Elastic-plastic and elastic-secondary creep behavior models are employed in this study. Slight variations of the parent or base metal (BM) inelastic properties are assumed for the weld (WM), while the HAZ metal was modeled with average properties of the weld and base metals. In every case the elastic properties are identical. Under elastic-plastic conditions given in Equation (3) $2\frac{1}{4}$ CrMoV steel is used as the BM and has the following room temperature properties:

$$E = 175 \text{ Gpa}, \qquad \nu = 0.3, \qquad \sigma_0 = 168 \text{ MPa}, \qquad \alpha = 2.2, \qquad m = 5 \qquad (15)$$

At $T = 538\,^\circ C$, elastic-secondary creep conditions given in Equation (6) are assumed, and the material constants for the BM are given as

$$E = 160 \text{ GPa}, \qquad \nu = 0.3, \qquad A = 2.0 \times 10^{-17} \text{ MPa}^{-n}\text{hr}^{-1}, \qquad n = 4.7 \qquad (16)$$

The material property mismatch, χ_M, is defined as the weld-to-base metal ratio of any material property M, for example $\chi_A = A_{WM}/A_{BM} = 10$. In many of the cases studied here, the WM is more strain compliant than the BM; we say in this case that the properties are *undermatched* in the sense of strength. The converse case is *overmatched*. Property mismatches are varied concurrently with the thickness of the HAZ, t and the eccentricity or distance of the crack plane from the center of the HAZ, e. For positive eccentricity the crack tends to be embedded within the WM, whereas for increasing negative eccentricity, the crack tends to be embedded in the BM, depending on the thickness of the HAZ. In Figure 1, the eccentricity shown is negative since the crack lies in the BM. If $e = t = 0$, there is no HAZ and the crack lies on the WM-BM interface. If $e \neq 0$ but $t = 0$, the crack runs through the middle of the HAZ.

Visualizations of the time-dependent effective stress fields in creep were obtained for a variety of models. Some are illustrated in Figure 3. Elastic matching results in initially symmetric crack tip stress fields in all cases, but the steady state effective stress distribution for creep is non-symmetric across the interface due to the inelastic property mismatch and a near-tip shear stress exists near the crack plane. The magnitude of this shear stress is larger in the more inelastically compliant material (i.e., the HAZ and/or the WM region). Generally, the variation of effective stress across the interface increases with higher mismatch of inelastic properties. The accumulation of creep strain in the direction of the applied load (vertical-axis) is shown in Figure 4.

Figure 5 presents the singularity amplitude $C(t)$ normalized by the steady state creep amplitude C^* for the homogenous BM case under steady state creep conditions, labeled as C^*_{BM}, for several inelastic mismatch combinations in bimaterial models. In Figure 5, the eccentricity

Figure 3. Effective stress distribution in C(T)-specimens under creep conditions at $T = 538\,^\circ$C; (row 1) homogeneous base metal (BM), (row 2) bimaterial (BM-WM), (row 3) weldment with blended HAZ, (row 4) weldment with functionally graded HAZ, and (fifth row) eccentric bimaterial speciments. Each weldment specimen features an inelastic mismatch of $\chi_A = 100$ and $\chi_n = 1$. For each specimen, the effective stress field is shown at various times: (column 1) $t \ll t_{T_{WM}}, t_{T_{BM}}$, (column 2) $t \approx t_{T_{WM}}$, (column 3) $t \approx t_{T_{BM}}$, and (column 4) $t \gg t_{T_{WM}}, t_{T_{BM}}$.

Figure 4. Opening mode creep strain distribution in C(T)-specimens under creep conditions at $T = 538$ °C: (row 1) homogeneous base metal (BM), (row 2) bimaterial (BM-WM), (row 3) weldment with blended HAZ, (row 4) weldment with functionally graded HAZ, and (fifth row) eccentric bimaterial specimens. Each weldment specimen features an inelastic mismatch of $\chi_A = 100$ and $\chi_n = 1$. For each specimen, the effective stress field is shown at various times: (column 1) $t \approx t_{T_{WM}}$, (column 2) $t_{T_{WM}} < t < t_{T_{BM}}$, and (column 3) $t \approx t_{T_{BM}}$.
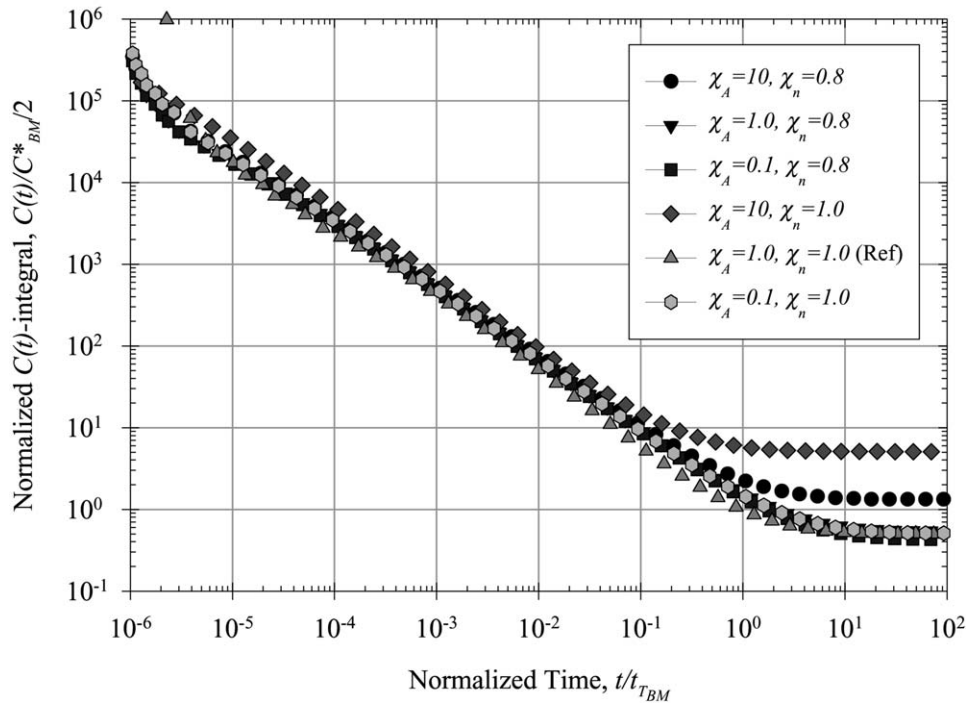
Figure 5. $C(t)$-integral for various bimaterial models ($e = t = 0$) with inelastic mismatches in strain hardening coefficient, A, and exponent, n. $T = 538\,°C$ for each case.

and HAZ thicknesses are both zero, so this is a true bimaterial crack model ($e = t = 0$). Curves for each of the equivalent domain integrals resemble the shape of the homogeneous BM case. For cases in which $\chi_A = 10$, the predicted steady state domain integrals are at least two times those of the other cases. For cases where the WM is more creep compliant than the BM (i.e., $\chi_A > 1.0$), the transition time between small scale and steady state creep conditions is higher than for $\chi_A < 1.0$. For each of the material mismatch cases for bimaterials, the resulting J and C^* predictions were observed to nearly follow the geometric mean of the corresponding J and C^* values of the two material constituents in the homogeneous case.

For increasing e and with $t = 0$ (no HAZ), the crack plane is distanced further from the interface. The crack tip is more deeply embedded within the weld metal, and J and C^* converge to J_{WM} and C^*_{WM}, respectively. The results of the elastic-plastic bimaterial models are normalized by the J-integral for the homogenous base metal case, JBM, and are shown in Figure 6. This convergence behavior is also observed for models with heat affected zones. Figure 7 illustrates elastic-plastic weldment models with a transition layer or HAZ of various levels of thickness, with $e = 0$. In this case, the properties of the HAZ are median properties of the WM and BM. The domain integral values exponentially approach J_{HAZ} and C^*_{HAZ}, respectively, as t increases. By increasing t or e, the discontinuous material property boundaries are further separated from the crack plane. In other words, the degree of homogeneous material near the crack tip along the path increases with increasing t or e. Crack tip stress, strain and displacement fields become increasingly similar to those of the corresponding homogenous HRR field. As a result, the crack tip driving force parameters approach those of the respective homogeneous cases.
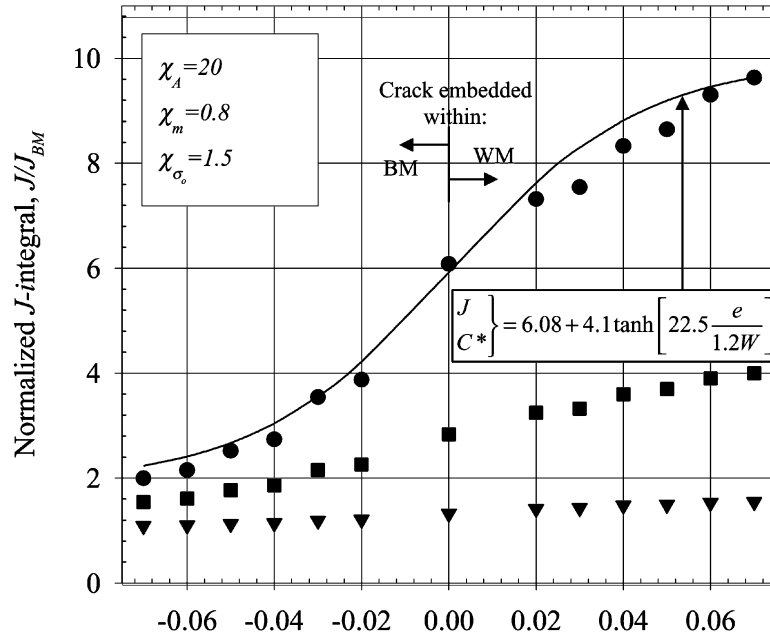
Figure 6. Variation of the *J*-integral with crack plance eccentricity for various plastic material property mismatches at room temperature. For each case, there is no HAZ, i.e., $t = 0$. The BM properties are identical in each model: as *e* decreases, J/J_{BM} approaches unity.
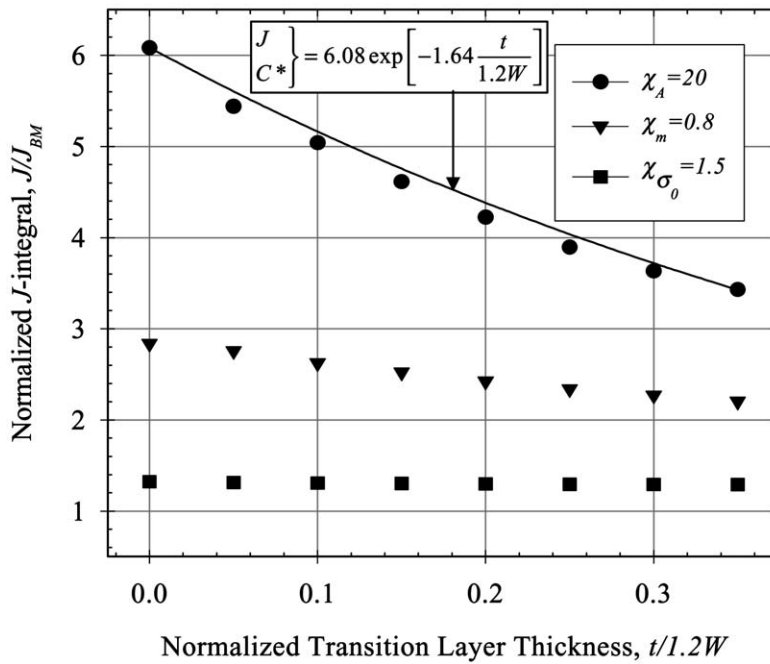
Figure 7. Variation of the *J*-integral with transition layer thickness for various plastic material property mismatches at room temperature. For each case, the initial crack plane is along the centerline of the HAZ, i.e., $e = 0$.

The resulting variation of the parameters for the graded bimaterial for $e = 0$ can be related via a simple power law expression. Generally, the fracture parameters can be approximately fit with the exponential form

$$\left. \begin{array}{c} J \\ C^* \end{array} \right\} = b(\chi) \exp\left(-D(\chi) \frac{1}{1.2W} \right) \right|_{e=0}, \tag{17}$$

where b and D are obtained via regression analysis. Function b takes on units of the fracture parameters, J (MPa-mm or J/mm^2) or C^* (MPa-mm/hr or J/mm^2-hr), while D is dimensionless The parameter b is usually bounded by the values of the fracture parameters that pertain to the identical crack in each of the homogeneous constituents of the bimaterial pair, i.e.,

$$b \in \left[\left\{ J_{BM}, C^*_{BM}, t_{T_{WM}} \right\}, \left\{ J_{WM}, C^*_{WM}, t_{T_{BM}} \right\} \right] \tag{18}$$

Here, $t_{T_{BM}}$ and $t_{T_{BM}}$ are the transition times from small scale to extensive steady state creep conditions in homogeneous WM and BM specimens, respectively. Moreover, b in the case $t > 0$ is close to the geometric mean of the fracture parameters for the homogeneous bodies, i.e.,

$$b \approx \sqrt{J_{BM} J_{WM}} \quad \text{or} \quad b \approx \sqrt{C^*_{BM} C^*_{WM}} \tag{19}$$

Also, $t_T \approx \sqrt{t_{T_{BM}} t_{T_{BM}}}$. If interested in the limiting range $t \to 0$, we can quantify b based on the results of the trivial bimaterial model.

If a relation with respect to crack plane eccentricity is sought without a HAZ ($t = 0$), then the form of Equation (17) can be slightly altered and t can be replaced with e in, i.e.,

$$\left. \begin{array}{c} J \\ C^* \end{array} \right\} = \left(b_e(\chi) + c_e(\chi) \tanh\left[d_e(\chi) \frac{e}{1.2W} \right] \right) \right|_{t=0} \tag{20}$$

4.2. BIMATERIAL INTERFACES

In weldments, grading of mechanical properties arises from the fusion process. During welding, contact between the liquefied weld metal and the base metal leads to partial melting of the base metal. This back-welding of BM allows some intermingling of the two materials and columnar grain coarsening. This process inherently creates a new material section known as the heat-affected zone. The thickness of this region is controlled by weld temperature, weld time, and other factors. Historically, fracture investigators assume homogeneity of the HAZ and apply a quasi-'rule of mixtures' to obtain these properties. We denote these cases as 'median' models since the intermediate layer has material properties that are a simple blend of the neighboring materials, as shown in Figure 8a.

Some fracture studies more accurately depict weldments by grading material properties through the transition layer; however, they limit consideration typically to linear property variation. Spatial dependence of yield strength properties is incorporated in only a very small number of studies. In this study, we grade the hardening coefficients and exponent of the HAZ. It is reasonable to assume that the material behavior at each of the HAZ boundaries must match those of the homogeneous weld and base metals. We replace sharp property variations with continuous functions, as depicted in Figures 8b and 9. Micro-hardness tests of welded specimens show that the variation in Vickers hardness changes nearly linearly between base
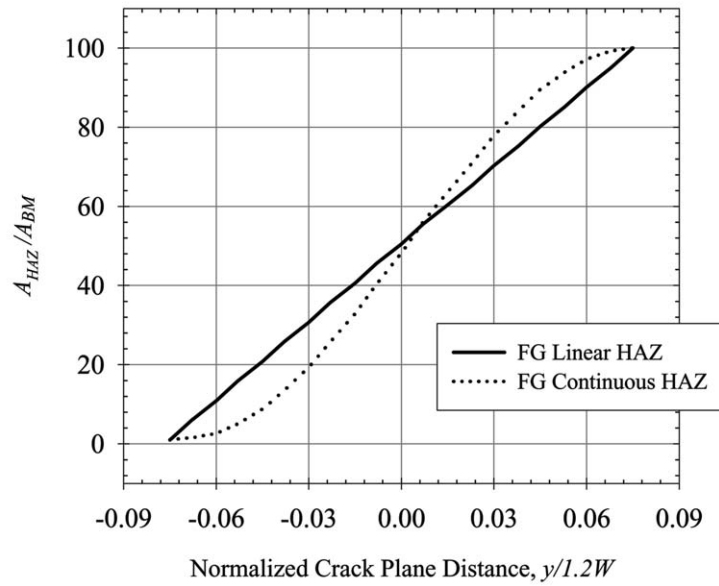
(a)
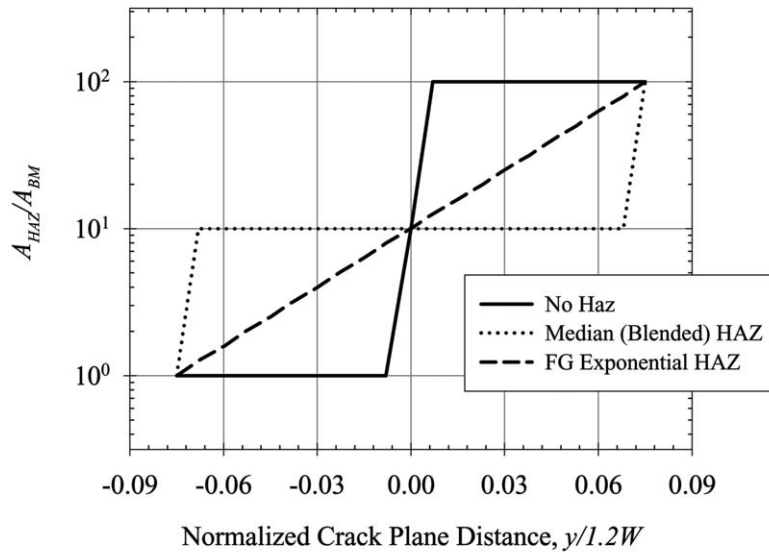
(b)

Figure 8. Prescribed spatial dependence for strain hardening coefficients for functionally graded (FG) and 'median' HAZ region. $\chi_A = 100$, $\chi_n = 1$ and $t/1.2W = 0.15$, and $e = 0$ for each case.

and weld metal regions (Miyazaki et al., 1993). This corresponds to linear yield strength variation through the HAZ, ranging from BM to WM properties at each respective interface. These indentation profiles can be combined with the Ramberg-Osgood power law expression to indicate that the strain hardening coefficient varies exponentially across the HAZ under the assumption that the strain hardening exponent is fixed. This argument is extended here to model a gradient of the creep coefficient, $A_{HAZ}(y)$, assuming that the creep exponent is fixed through the HAZ; such models have been simulated under identical boundary conditions
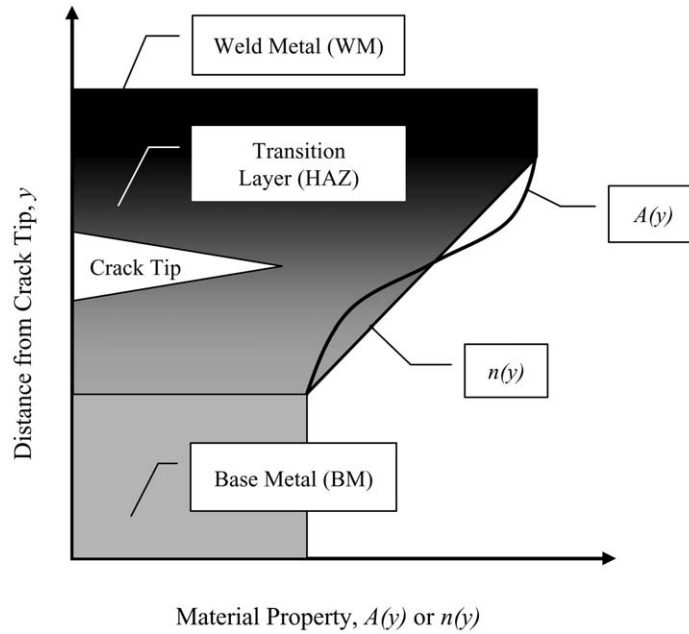
Figure 9. Inelastic material property spatial variation in functionally graded transition layers. For each case, $e = 0$.

Table 1. Resultant fracture parameters for homogeneous, bimaterial, and weldment models. $\chi_A = 100$ and $\chi_n = 1$ where applicable. For each case, $e = 0$.

Model Description	Normalized transition Time, $t_T / t_{T_{BM}}$	Normalized C*-Integral, C^* / C^*_{BM}
Homog. Base Metal	1.000	1.000
Homog. Weld Metal	0.010	100.000
Homog. HAZ Metal	0.100	10.000
Bimaterial (No Haz)	0.022	45.965
Median HAZ	0.033	29.452
FG Linear HAZ	0.037	25.994
FG Exponential HAZ	0.053	18.386
FG Continuous HAZ	0.049	19.135

and intermediate thickness levels. Figure 10 shows the resulting $C(t)$-integral of models with HAZs. These are normalized by the C^*-integral for the BM homogenous case under steady state creep conditions, C^*_{BM}. The value of C^* is lower for cases with functionally graded intermediate layers than median property models. Table 1 summarizes this trend.

Recall that median HAZ properties correspond to direct averages of properties of the WM and BM materials. When the thickness t of the HAZ is decreased, the graded and median model predictions converge. This is shown in Figure 11. Conversely, as the thickness increases these diverge. The C^* value is always lower in cases with functionally graded HAZ layers than for median property models.
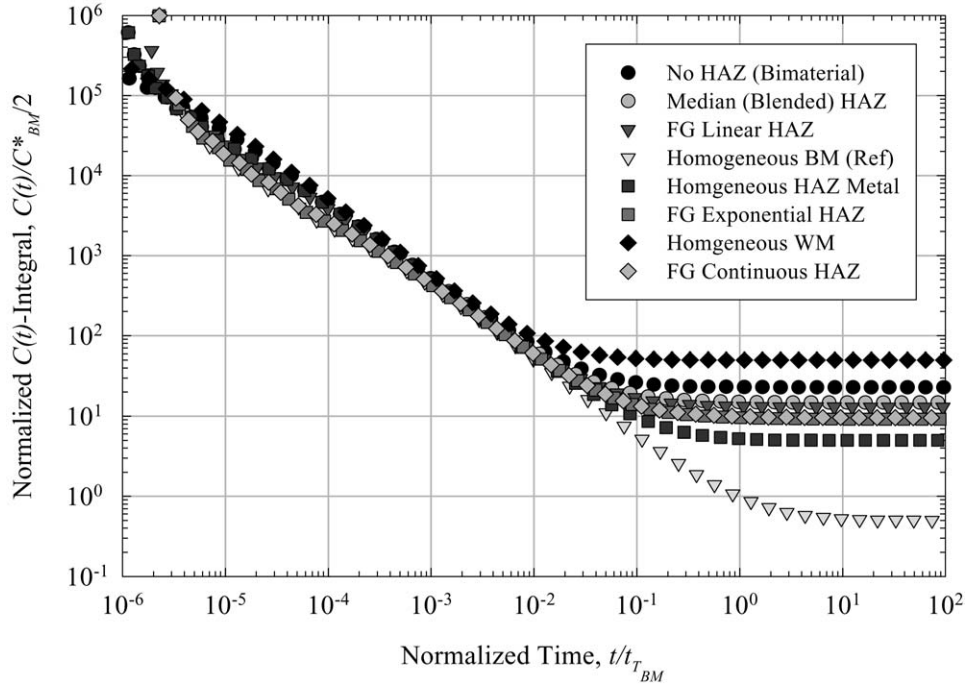
Figure 10. Comparison of $C(t)$-integral results for models with various functionally graded (FG) HAZ sections under creep conditions at $T = 538\ °C$. $\chi_A = 100$, $\chi_n = 1$, and $e = 0$ for each case.

4.3. MODE MIXITY

Cracks propagate along a path of least material resistance for a given crack driving force. This observation is critical since cracks in practical applications are seldom exposed to purely Mode I loading conditions. Moreover, the nature of bimaterial crack tip stress fields is inherently of mixed mode character. Mixed mode conditions in the presence of stress triaxiality lead to crack bifurcation and/or kinking. Numerous criteria attempt to correlate mixed mode crack propagation behavior found from fracture experiments to stress, strain, or displacement fields obtained from finite element models.

The traction experienced at a crack tip in a bimaterial interface crack between linear elastic constituents can be described by a set of local solid phase angles. Each of these quantities represents the ratio of in-plane shear-to-normal tractions and out-of-plane shear-to-normal tractions, i.e.,

$$\tan \psi = \frac{\Im\{\mathbf{Kr}^{i\varepsilon}\}}{\Re\{\mathbf{Kr}^{i\varepsilon}\}}, \quad \cos \phi = \frac{K_{\mathrm{III}}}{\sqrt{|\mathbf{K}|^2 + K_{\mathrm{III}}^2}}, \tag{21}$$

where $\mathbf{K}$ is the complex stress intensity factor. For Mode I loading of an elastic bimaterial, the in-plane crack tip mode mixity parameter, phase angle ψ, is uniquely described by ε, the bimaterial constant given by Williams (1959). The out-of-plane phase angle, ϕ, is irrelevant in two-dimensional analyses. In the case of a stationary creep crack, these phase angles pertain only in the limit of short times after initial loading, i.e., $t \to 0^+$.

Subsequent investigations applied ψ to predict the fracture energy and the direction of crack extension in bimaterial problems under small-scale yielding (SSY) conditions for which

(a)

(b)
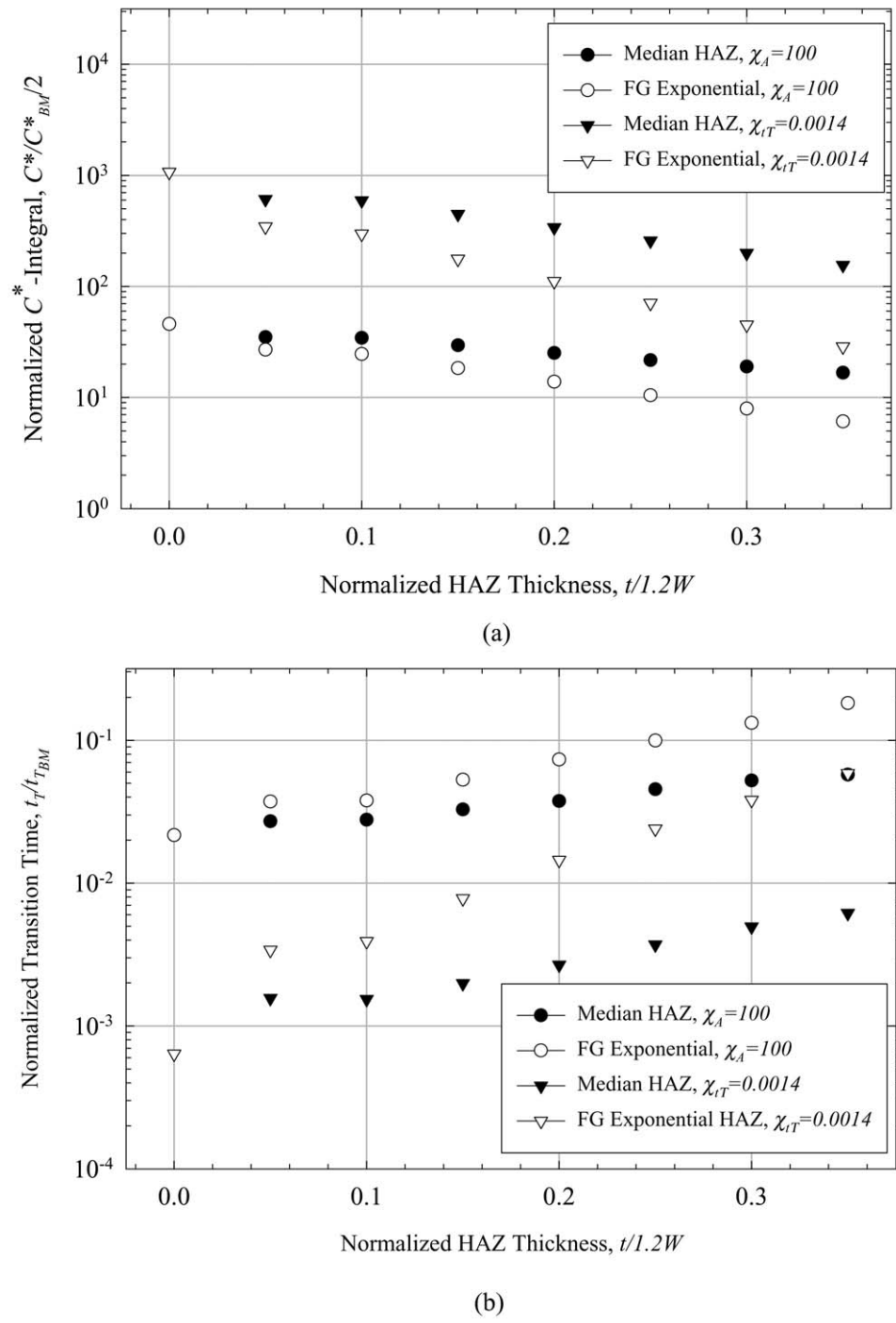
Figure 11. Dependence on HAZ thickness under creep conditions at $T = 538\ °C$ of (a) C^*-integral and (b) transition time. For each case, $E = 0$.

the crack tip is constrained by a linear elastic field. Under SSY conditions and for elastically matched models, the in-plane local phase angle, ψ, is proportional to the plastic mode mixity parameter, M_p, defined in Equation (14). Shih (1974) showed that the mixed-mode HRR fields for cracks in homogeneous elastic-plastic materials are parameterized by M_p under SSY conditions. Since M_p can be directly linked to ψ for the elastic and SSY cases, but can also provide meaningful information for arbitrary nonlinear material behavior under large scale yielding, we use M_p here, computed at a distance $r/W = 0.004$ directly ahead of the crack tip. Correlations of these crack tip parameters to crack propagation trajectories can only be made in connection with analogous experiments.

Elastically matched cases ($E_{WM} = E_{BM}$ and $\nu_{WM} = \nu_{BM}$) for bimaterial interface cracks subjected to remote Mode I conditions exhibit no shear along the crack plane in the absence of plasticity or creep deformation. As such, $M_p = 0$. Conversely, when the material constituents on either side of the crack are not elastically matched, significant crack plane shear is present upon initial loading and non-zero M_p is always obtained. This phenomenon occurs for any type of nonlinear material behavior. Li et al. (1988) showed that the singular crack tip fields for stationary cracks subjected to remote Mode I conditions are of mixed mode character and the magnitude of the shearing mode contribution increases with increase of property mismatch.

The transition times of stationary cracks in elastically matched bimaterials with distinct creep properties lie between those of the base and weld metals, t_{TWM} and t_{TBM}. The near-tip mode mixity during this transient behavior is reflected by M_p for models with transition layer thickness, t, that make use of blended, functionally graded material properties. The gradient function used throughout the remainder of this study is the exponential relation shown in Figure 8b.

Since the weld material occupies the upper region in the cracked specimen model, positive local M_p indicates that the crack is likely to grow towards the more creep strain compliant constituent, the WM in this case. This is a recurring result for each simulation. In Figures 12 and 13, models with a finite HAZ thickness predict local M_p values that favor crack bifurcation in the direction of the weld metal. Modeling weldments with 'median' HAZs lead to lower values of shear stresses near the crack tip. When the fracture specimen is simulated with a graded section of some specified thickness, M_p is increased. Once extensive steady state creep conditions (EC) are reached in the base metal, M_p becomes constant.

This procedure is repeated for specimens that feature eccentrically located cracks. Figure 14 indicates that for any level of eccentricity, the local M_p is positive. When the crack is located within the BM ($e < 0$), M_p increases by at least a factor of two and saturates at times closer to tTBM. The level of the mismatch also influences M_p, as shown in Figure 15.

5. Conclusions

By conducting a parametric study of stationary cracks subjected to non-linear and time-dependent material behavior, the influence of the crack plane-to-interface distance on the crack tip driving forces was studied. Transition layers between bimaterials have been included in this work; it was demonstrated that the severity of the stress and strain fields ahead of the crack tip and along the interface is reduced relative to the distinct bimaterial interface case. By computing a near tip mode mixity factor M_p, we infer the likelihood of crack bifurcation direction.
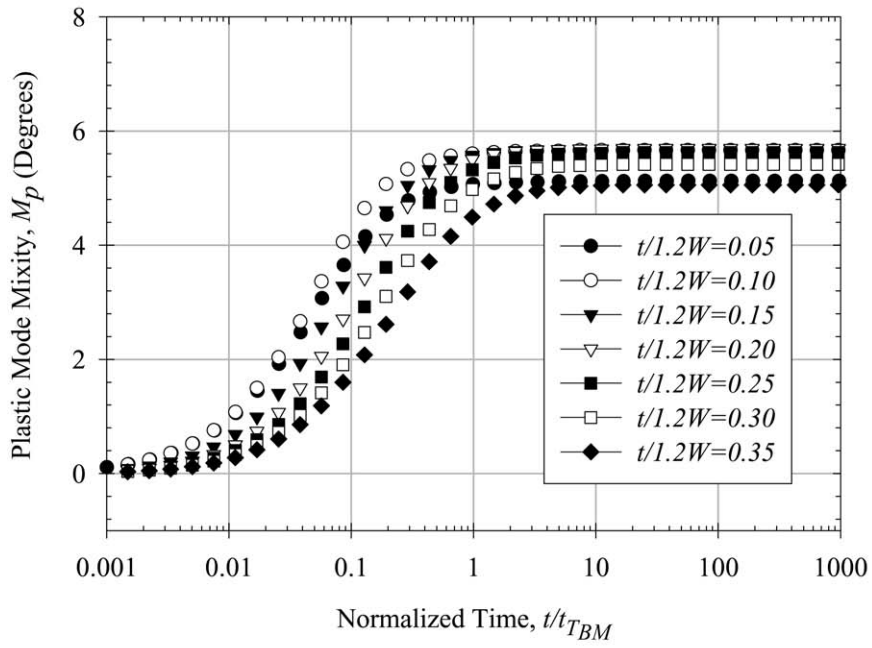
(a)
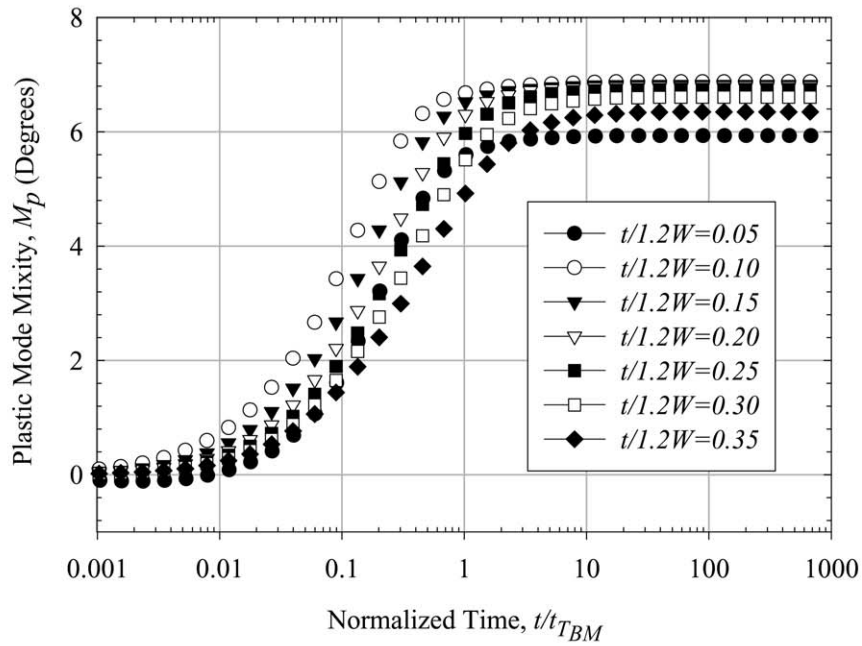
(b)

Figure 12. Convergence of mode mixity parameter M_p for models under creep conditions at $T = 538$ °C for cases with (a) median HAZs and (b) functionally graded HAZs. $\chi_A = 100$, $\chi_n = 1$, and $e = 0$ for each case.
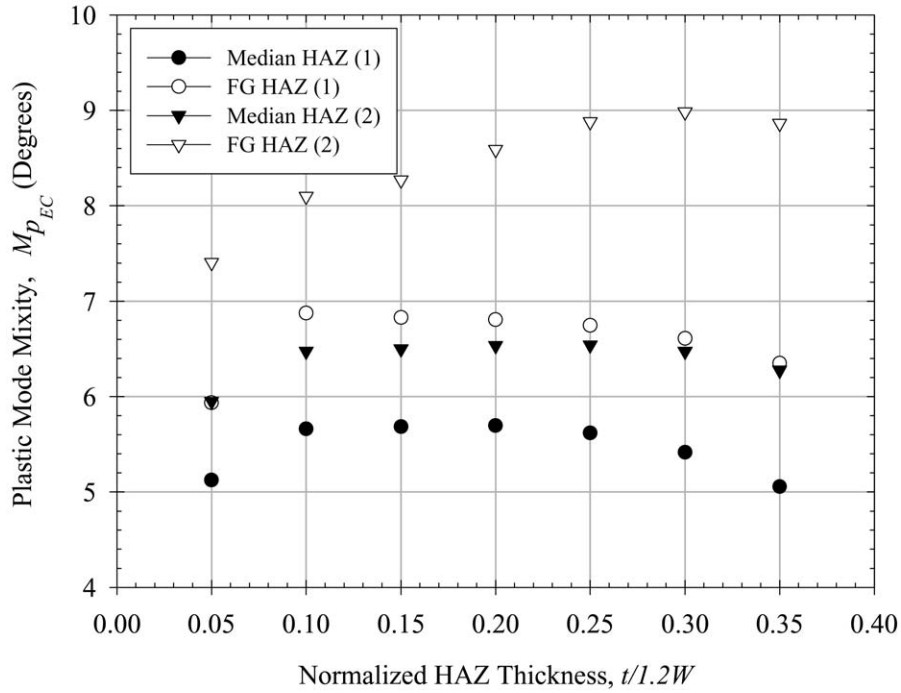
Figure 13. Mode mixity parameter M_p for mismatched models under extensive steady state creep conditions (EC) at $T = 538\,°C$ for cases with (a) $\chi_A = 100$, $\chi_n = 1$ and (2) $\chi_{tT} = 0.0014$. For each case $e = 0$.
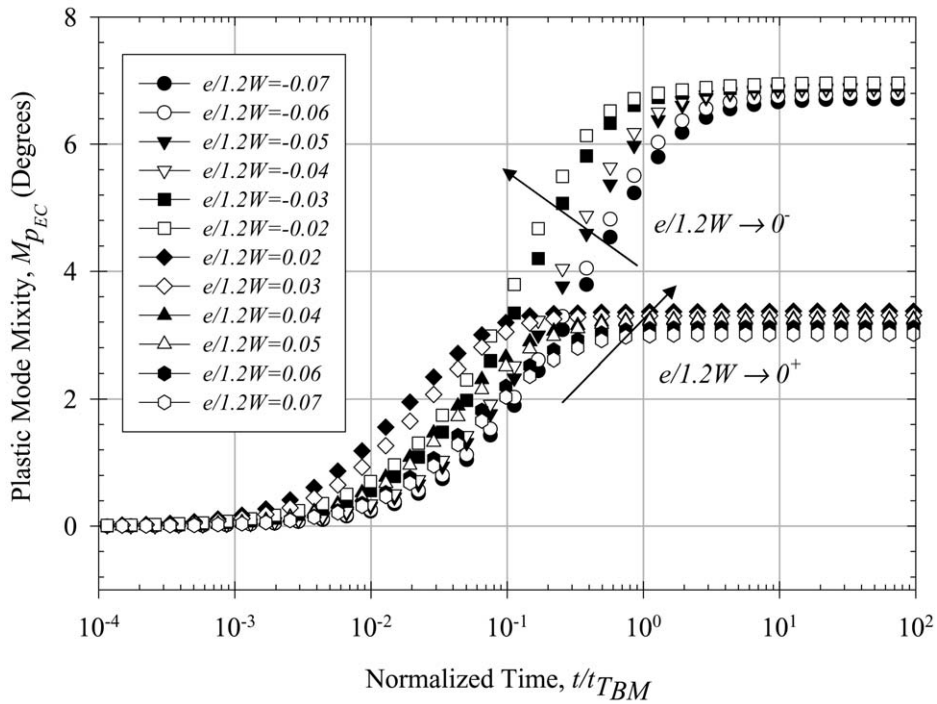
Figure 14. Convergence of mode mixity parameter M_p for eccentric models under creep conditions at $T = 538\,°C$. $\chi_A = 100$, $\chi_n = 100$, and $t = 0$ for each case.
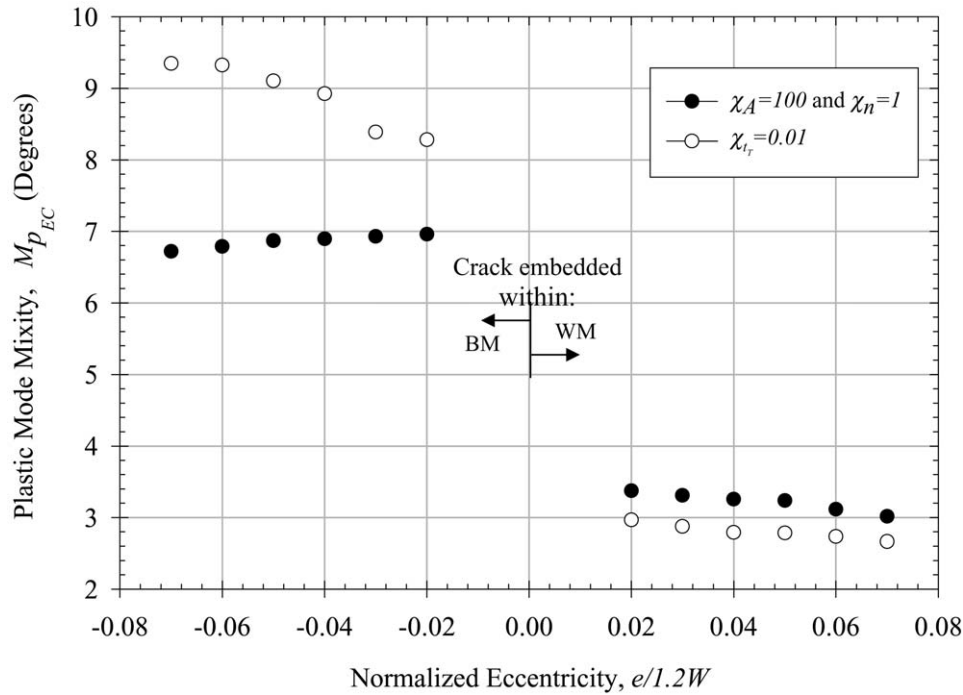
Figure 15. Mode mixity parameter M_p for mismatched models under extensive steady state creep conditions (EC) at $T = 538\,°\mathrm{C}$. For each case $t = 0$.

In addition to material properties, crack location relative to interfaces and width of a transition layer of intermediate properties both have an effect on the evolution and steady-state values of the asymptotic stress and strain fields near the crack tip. They affect the approximation of the fracture parameters J, C^*, and t_T, and the local mode mixity parameter, M_p. From the parametric analysis of several inelastic property mismatches for various crack plane-to-interface geometries, the behavior of the near-tip stress fields and crack tip parameters have been examined. Regardless of the type of material mismatch, the variation of the driving force parameters J and C^* across a range of transition layer thickness or eccentricities can be curve fit, as can the transition time from small scale to extensive, steady state creep of cracked specimens. The predicted parameters are typically bounded by those of the same crack in each of the homogenous constituents. For trivial, perfect bimaterial cases, the fracture parameters approximately follow the geometric mean of those of the same crack in homogeneous constituents. Variation in either the eccentricity or the thickness of the transition layer (e.g. the weldment interface(s) is moved farther away from the crack tip) facilitates noteworthy variations in the stress and strain fields. The predicted behavior begins to approximate homogeneous behavior of the base or weld metal as the transition layer thickness increases. Our results are consistent with these limiting behaviors.

The mode mixity parameter M_p exhibits slight changes with respect to specimen dimensions and material property mismatch as well; M_p predicts the maximum Mode I direction along the crack plane for cracks in homogeneous bodies with remote Mode I loading. For the eccentric and HAZ thickness cases studied, crack bifurcation (if cracks were allowed to propagate) is indicated towards the more compliant of the constituents. Effective stress disparities at graded interfaces are smaller than those for blended interfaces. These correspond

to estimates of fracture parameters J, C^*, or, t_T, that are closer to the geometric mean of the bimaterial analogy (a WM-BM model).

The near tip shear stresses, which can cause crack tip bifurcation in perfect bimaterial case, are generally reduced for the eccentric crack. We can propose how a crack might propagate in a weldment by considering a range of bimaterial cases with various e values and initial crack lengths. Consider, for example, an interface crack ($e = 0$) with length a, and inelastic property mismatch χ_M. Experiments involving elastic-plastic materials show that the crack is likely to extend into the more plastic strain compliant material (Shukla, 2001; Sorensen and Horsewell, 2001; Varias et al., 1999), thus creating a kinked crack. Crack tip mode mixity decreases when the interface is further away from the initial crack plane, so the near tip behavior resembles that of homogeneous crack tip conditions. Eccentric crack models showed decreased crack tip mode mixity relative to the non-eccentric case. As a consequence, the mixed mode crack tip stress fields that have promoted crack kinking from the interface may relax and cause the crack to turn and meander parallel to the interface. Ultimately, this must be supported by crack propagation analyses and experiments.

These results for J and C^* can be combined with fracture toughness (material resistance) properties to predict CCG rates; as a caveat, future numerical studies should incorporate propagation along a direction that is controlled by the evolution of the near tip stress and strain fields. Since no generalized analytical solution exists for the variation of the stress, strain, and displacement fields near the interface crack tip for time-dependent creep conditions, the results of this study can only be confirmed and extended by performing growing crack analyses and in connection with experiments. Once solutions of J and C^* are made from load-line deflection results obtained from growing crack analyses or experiments carried out with the identical conditions as the models presented in this study, the crack tip parameters that were developed here can be correlated with crack growth rates.

Acknowledgements

References

Bassani, J.L. and McClintock, F.L. (1981). Creep Relaxation of Stress Around a Crack Tip. *International Journal of Solids and Structures* **17**, 79–89.

Biner, S.B. (1998). Characteristics of Interface Cracks. *Materials Science and Engineering* **A 244**, 233–249.

Burstow, M.C., Howard, I.C. and Ainsworth, R.A. (1998). The Influence of Constraint on Crack Tip Stress Fields in Strength Mismatched Welded Joints. *Journal of Mechanics and Physics of Solids* **46**(5), 845–872.

Dundurs, J. (1969). Edge-Bonded Dissimilar Orthogonal Elastic Wedges Under Normal and Shear Loading. *Journal of Applied Mechanics* **36**, 650–652.

Ehlers, R. and Riedel, H. (1991). *A Finite Element Analysis of Creep Deformation in a Specimen Containing a Macroscopic Crack*. Advances in Fracture Research ECF-5, e.D. Francois et al. Oxford, Pergamon.

Francis, M. and Rahman, S. (2000). Probabilistic Analysis of Weld Cracks in Center-Crack Tension Specimens. *Computers and Structures* **76**, 483–506.

Hutchinson, J.W. (1968). Plastic Stress and Strain Fields at a Crack Tip. *Journal of Mechanics and Physics of Solids* **16**, 337–347.

Hutchinson, J.W. (1968). Singular Behavior at the End of a Tensile Crack Tip in a Hardening Material. *Journal of the Mechanics and Physics of Solids* **16**, 13–31.

Kim, Y.-J. and Schwalbe, K.-H. (2001). Mismatch Effect on Plastic Yields in Idealised Weldments II. Heat Affected Zone Cracks. *Engineering Fracture Mechanics* **68**, 183–199.

Landes, J.D. and Begley, J.A. (1976). A Fracture Mechanics Approach to Creep Crack Growth. *Fracture Analysis, ASTM STP 590*. Philadelphia, PA, ASTM, 128–148.

Liaw, P.K., Saxena, A. and Schaefer, J. (1989). Estimating Remaining Life of Elevated-Temperature Steam Pipes-Part I. Materials Properties. *Engineering Fracture Mechanics* **32**(5), 675–708.

Li, F.Z., Needleman, A. and Shih, C.F. (1988). Characterization of Near Tip Stress and Deformation Fields in Creeping Solids. *International Journal of Fracture* **36**, 163–186.

Luo, X.F. and Aoki, S. (1992). Crack Growth on Elastic-Plastic Bimaterial Interfaces. *International Journal of Fracture* **57**, 365–379.

Miyazaki, N., Nakagaki, M., Sasaki, T., Sakai, T. and Munakata, T. (1993). Finite Element Analysis of Stable Crack Growth in Inhomogeneous Materials. *JSME International Journal, Series A: Mechanics and Material Engineering* **36**(4), 361–366.

Moran, B. and Shih, C.F. (1987). Crack Tip and Associated Domain Integrals from Momentum and Energy Balance. *Engineering Fracture Mechanics* **27**(6), 615–642.

Nikbin, K.M., Webster, G.A. and Turner, C.E. (1976). Relevance of Nonlinear Fracture Mechanics to Creep Crack Growth. *Fracture Analysis, ASTM STP 601*, 47–62.

Rice, J.R. (1968). Mathematical Analysis in the Mechanics of Fracture.' *Fracture: An Advanced Treatise*. H. Liebowitz, Editor. New York, NY, Academic Press. **2**, 191–311.

Rice, J.R. (1968). A Path Independent Integral and the Approximate Analysis of Strain Concentration by Notches and Cracks. *Journal of Applied Mechanics* **35**, 379–386.

Rice, J.R. and Tracey, D.M. (1969). On the Ductile Enlargement of Voids in Triaxial Stress Fields. *Journal of Mechanics and Physics of Solids* **17**, 102–217.

Rice, J.R. and Rosengren, G.F. (1968). Plane Strain Deformation Near a Crack Tip in a Power-Law Hardening Material. *Journal of the Mechanics and Physics of Solids* **16**, 1–12.

Riedel, H. and Rice, J.R. (1980). Tensile Cracks in Creeping Solids. *Fracture Mechanics, ASTM STP 700*. P.C. Paris, Editor. Philadelphia, PA, ASTM: 112–130.

Saxena, A. (1998). *Nonlinear Fracture Mechanics for Engineers*. New York, CRC Press.

Saxena, A. (1986). Creep Crack Growth Under Non-Steady-State Conditions. *Fracture Analysis, ASTM STP* **905**, 185–201.

Segle, P., Andersson, P. and Samuelson, L. (1998). A Parametric Study of Creep Crack Growth in Heterogeneous CT Specimens by Use of Finite Element Simulations. *Materials at High Temperatures* **15**(2), 63–68.

Shih, C.F. (1974). Small Scale Yielding Analysis of Mixed Mode Plane-Strain Crack Problems. *Fracture Analysis, ASTM STP 560*, 187–210.

Shih, C.F., Moran, B. and Nakamura, T. (1986). Energy Release Rate Along a Three-Dimensional Crack Front in a Thermally Stressed Body. *International Journal of Fracture* **30**, 79–102.

Shih, C.F. and Asaro, R.J. (1989). *Journal of Applied Mechanics*, 763–779.

Shih, C.F. and Asaro, R.J. (1988). Elastic-Plastic Analysis of Cracks on Bimaterial Interfaces: Part I-Small Scale Yielding. *Journal of Applied Mechanics* **55**(2), 299–316.

Shih, C.F., Asaro, R.J. and O'Dowd, N.P. (1991). Elastic-Plastic Analysis of Cracks on Bimaterial Interfaces: Part III - Large Scale Yielding. *Journal of Applied Mechanics* **58**(2), 450–462.

Shih, C.F., Asaro, R.J. and O'Dowd, N.P. (1993). Elastic-Plastic Analysis of Cracks on Bimaterial Interfaces: Interfaces with Structure. *Materials Science and Engineering* **A162**, 175–192.

Shukla, A. (2001). High-Speed Fracture Studies on Bimaterial Interfaces Using Photoelasticity. *Journal of Strain Analysis for Engineering Design* **36**(2), 119–142.

Sorensen, B.F. and Horsewell, A. (2001). Crack Growth Along Interfaces in Porous Ceramic Layers. *Journal of the American Ceramic Society* **84**(9), 2051–2059.

Tada, H., Paris, P.C. and Irwin, G.R. (1985). *The Stress Analysis of Cracks Handbook (2nd Ed.)*. St. Louis, Paris Productions, Inc.

Tvergaard, V. (1984). On the Creep Constrained Diffusive Cavitation of Grain Boundary Facets. *Journal of Mechanics and Physics of Solids* **32**(5), 373–393.

Varias, A.G., Mastorakos, I. and Aifantis, E.C. (1999). Numerical Simulation of Interface Crack in Thin Films. *International Journal of Fracture* **98**(3), 197–207.

Williams, M.L. (1959). The Stresses Around a Fault or Crack in Dissimilar Media. *Bulletin of the Seismological Society of America* **49**(2), 199–204.